

Edge-Bridged Octahedral Tungsten–Oxygen–Chlorine Clusters: Synthesis and Characterization of Two D_{3d} -Symmetric $[\text{W}_6\text{O}_6\text{Cl}_{12}]^{2-}$ Isomers and $[\text{W}_6\text{O}_7\text{Cl}_{11}]^{3-}$

Nathan R. M. Crawford and Jeffrey R. Long*

Department of Chemistry, University of California, Berkeley, California 94720-1460

Received December 6, 2000

Initial access to the chemistry of hexanuclear tungsten oxohalide clusters is provided through the reduction of WOCl_4 with bismuth metal at 360 °C. Reactions targeting $\text{W}_6\text{O}_6\text{Cl}_{10}$ produce an amorphous black solid, which, upon treatment with concentrated aqueous HCl, releases the edge-bridged octahedral cluster $[\alpha\text{-W}_6\text{O}_6\text{Cl}_{12}]^{2-}$ into solution. The cluster exhibits a D_{3d} -symmetry structure in which the six oxygen atoms bridge the edges between two opposing triangular faces of a trigonally compressed W_6 octahedron. Reactions incorporating additional bismuth metal yield a mixture of soluble clusters, including a 5:7 ratio of $[\alpha\text{-W}_6\text{O}_6\text{Cl}_{12}]^{2-}$ and another D_{3d} -symmetry isomer, $[\beta\text{-W}_6\text{O}_6\text{Cl}_{12}]^{2-}$. The latter species displays a different core structure, in which the six oxygen atoms are situated on the edges comprising two opposing triangular faces of a trigonally elongated W_6 octahedron. Isolated as the BuN^+ salts, the two isomers can be separated by a process relying on the differences in crystal morphology. Cyclic voltammetry of acetonitrile solutions shows two reversible one-electron reductions for each cluster, the α isomer being slightly more easily reduced. Density functional theory calculations indicate that the two isomers of $[\text{W}_6\text{O}_6\text{Cl}_{12}]^{2-}$ are nearly identical in energy, with the β isomer lying just 1.4 kcal/mol below the α isomer. The other major product isolated from the reaction with additional bismuth is $[\text{W}_6\text{O}_7\text{Cl}_{11}]^{3-}$, a cluster at least formally related to $[\beta\text{-W}_6\text{O}_6\text{Cl}_{12}]^{2-}$ by substitution of an O^{2-} ion for a core Cl^- ion. In acetonitrile solution, this cluster displays a single reversible one-electron reduction. It is anticipated that the reactions elaborated here will lead to a general method for synthesizing metastable metal oxohalide clusters.

Introduction

The halides of early second- and third-row transition metals in low oxidation states display a propensity for forming hexanuclear clusters based on an octahedral arrangement of metal atoms.¹ Niobium and tantalum halides tend to adopt structures with the edge-bridged octahedral geometry depicted in Figure 1, in which 16 valence electrons participate in metal–metal bonding. In contrast, molybdenum and tungsten halides tend to exhibit structures with a face-capped octahedral geometry, where 24 valence electrons are involved in the metal–metal bonding. Noteworthy exceptions to these generalizations have been observed in the structures of Nb_6I_{11} ,² featuring face-capped octahedral $[\text{Nb}_6\text{I}_8]^{3+}$ cluster cores with 19 metal-based valence electrons, and W_6Cl_{18} (see Figure 1),³ containing edge-bridged octahedral $[\text{W}_6\text{Cl}_{12}]^{6+}$ cluster cores with 18 metal-based valence electrons.

The edge-bridged octahedral cluster motif is also recognizable in many reduced niobium and molybdenum oxide phases, frequently as a component of some more condensed structure.^{1a,4} Analogous tantalum-containing phases are less common,⁵ and only a single compound featuring edge-bridged octahedral $[\text{W}_6\text{O}_{12}]^{2-}$ cluster cores has been structurally characterized.⁶ As

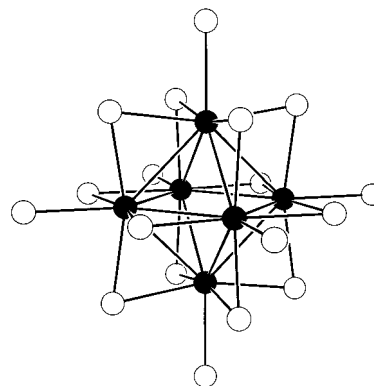


Figure 1. Structure of the edge-bridged octahedral W_6Cl_{18} cluster, as observed in $\text{W}_6\text{Cl}_{18}\cdot 4\text{Me}_2\text{SO}$.^{3b} Black and white spheres represent W and Cl atoms, respectively.

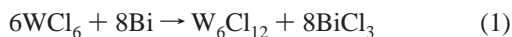
might be expected given the shared preference of the pure oxide and halide clusters, hexanuclear niobium and tantalum clusters with a mixture of oxygen and halogen ligands are also found to adopt this geometry. To date, phases have been identified as containing $[\text{Nb}_6\text{OCl}_{11}]^{1+}$,⁷ $[\text{Nb}_6\text{O}_n\text{Cl}_{12-n}]^{(4-n)+}$ ($n = 2-4$),⁸

- (1) (a) Simon, A. *Angew. Chem., Int. Ed. Engl.* **1988**, *27*, 159. (b) Perrin, A.; Perrin, C.; Sergent, M. *J. Less-Common Met.* **1988**, *137*, 241. (c) Lee, S. C.; Holm, R. H. *Angew. Chem., Int. Ed. Engl.* **1990**, *29*, 840. (d) Corbett, J. D. *J. Alloys Compd.* **1995**, *229*, 10. (e) Perrin, C. *J. Alloys Compd.* **1997**, *262–263*, 10. (f) Prokopuk, N.; Shriver, D. F. *Adv. Inorg. Chem.* **1999**, *46*, 1 and references therein.
- (2) (a) Simon, A.; von Schnering, H.-G.; Schäfer, H. *Z. Anorg. Allg. Chem.* **1967**, *355*, 295. (b) Imoto, H.; Simon, A. *Inorg. Chem.* **1982**, *21*, 308.
- (3) (a) Siepmann, R.; von Schnering, H.-G.; Schäfer, H. *Angew. Chem., Int. Ed. Engl.* **1967**, *6*, 637. (b) Zheng, Y.-Q.; Jonas, E.; Nuss, J.; von Schnering, H. G. *Z. Anorg. Allg. Chem.* **1998**, *624*, 1400.

- (4) (a) Torardi, C. C.; McCarley, R. E. *J. Am. Chem. Soc.* **1979**, *101*, 3963. (b) Lii, K.-H.; Wang, C. C.; Wang, S. L. *J. Solid State Chem.* **1988**, *77*, 407. (c) Lindblom, B.; Strandberg, R. *Acta Chem. Scand.* **1989**, *43*, 825. (d) Dronskowski, R.; Simon, A.; Mertin, W. *Z. Anorg. Allg. Chem.* **1991**, *602*, 49. (e) Köhler, J.; Svensson, G.; Simon, A. *Angew. Chem., Int. Ed. Engl.* **1992**, *31*, 1437 and references therein.
- (5) (a) Siegrist, T.; Cava, R. J.; Krajewski, J. *J. Mater. Res. Bull.* **1997**, *32*, 881. (b) Harbrecht, B.; Wagner, V.; Ritter, A. *Z. Anorg. Allg. Chem.* **1998**, *624*, 457. (c) Ritter, A.; Lydssan, T.; Harbrecht, B. *Z. Anorg. Allg. Chem.* **1998**, *624*, 1791.
- (6) Hibble, S. J.; McGrellis, S. A. *J. Chem. Soc., Dalton Trans.* **1995**, 1947.

$[\text{Ta}_6\text{O}_3\text{X}_9]^{1+}$ ($\text{X} = \text{Cl}, \text{Br}$),⁹ and $[\text{Nb}_6\text{O}_6\text{Cl}_6]^{1-10}$ cluster cores, with 16, 14, 14, and 13 metal-based valence electrons, respectively. A similar chemistry for hexanuclear molybdenum and tungsten oxohalide clusters has thus far failed to emerge.

Most of the aforementioned cluster phases are prepared by standard solid-state routes—stoichiometric reactions carried out at temperatures in excess of 700 °C. Early syntheses of binary molybdenum and tungsten halide cluster compounds proved less straightforward, however, involving disproportionation of some more oxidized form of the metal halide and suffering from poor yields.^{1f} More efficient preparations, wherein a metal halide is reduced by aluminum metal in a sodium tetrahaloaluminate melt, have since been developed.¹¹ And recently, a convenient, high-yield route to W_6Cl_{12} employing bismuth metal as a reductant was reported.¹²



Reaction 1 can be accomplished at temperatures as low as 335 °C,¹² suggesting the possibility of utilizing reactions of this type to gain some measure of kinetic control over the composition and perhaps even the structure of the cluster product. Herein, we convey the results of analogous reactions in which WOCl_4 is reduced with bismuth metal, providing an entry to tungsten oxochloride cluster chemistry.

Experimental Section

Preparation of Compounds. The reagents $\text{Na}_2\text{WO}_4 \cdot 2\text{H}_2\text{O}$ (Aldrich), HCl (Fisher), SOCl_2 (Aldrich), Bi (−100 mesh, Aldrich), Bu_4NBr (Aldrich), NaHCO_3 (Aldrich), and Et_4NCl (Aldrich) were used as purchased. Water was distilled and deionized with a Milli-Q filtering system. Pyrex ampules with dimensions i.d. \times o.d. \times l. = $10 \times 13 \times 200$ mm were employed. High temperature reactions were carried out in a 36-inch tube furnace equipped with a programmable temperature controller; the furnace temperature was generally ramped up at a rate of 1.5 °C/min.

WOCl_4 . The synthesis of this compound was adapted from two previously reported preparations.¹³ A boiling solution of $\text{Na}_2\text{WO}_4 \cdot 2\text{H}_2\text{O}$ (10.0 g, 30.4 mmol) in 30 mL of water was carefully added to a stirred 40 mL volume of boiling concentrated hydrochloric acid. A deep yellow precipitate formed immediately, and the solution was allowed to cool to room temperature. The precipitate was collected by filtration and washed with successive aliquots of water (3×5 mL) and ether (20 mL). The ensuing tacky solid (tungstic acid) was transferred using a plastic spatula into a dinitrogen-purged flask charged with 80 mL of SOCl_2 . A reflux condenser was attached to the flask, and nitrogen flow switched to a slow purge, with exhaust routed through a mineral oil bubbler followed by an acid-neutralizing trap. After the initial gas evolution subsided, the reaction mixture was stirred and heated at reflux for 8 h until gas evolution ceased. The clear, orange-red solution was reduced to dryness under vacuum. A liquid nitrogen trap and a gas

drying tower filled with NaOH pellets were employed during this process to protect the vacuum pump. The resulting orange residue was transferred to a sublimator under a dinitrogen atmosphere. Sublimation at 100 mTorr and 90 °C over the course of several days gave 8.99 g (87%) of product as orange-red needle-shaped crystals. Mp 210–212 °C; lit. 208–212 °C.

$(\text{Bu}_4\text{N})_2[\alpha\text{-W}_6\text{O}_6\text{Cl}_{12}]$. An ampule was charged with WOCl_4 (0.65 g, 1.9 mmol) and Bi (0.32 g, 1.5 mmol) in a dinitrogen atmosphere; the ampule was then evacuated and sealed. To ensure co-localization of the reactants at elevated temperatures, the ampule was placed in the tube furnace with the vacant end positioned in the center of the furnace and raised by a piece of glass wool. The furnace was heated at 200 °C for 2 h, and then at 360 °C for an additional 17 h. After cooling enough to handle, the ampule was repositioned such that the end not containing the solid reaction product was situated at the furnace opening. The tube was then reheated at 360 °C for 17 h in order to sublime away BiCl_3 . Upon cooling to room temperature, the ampule was broken open in air, and the black solid from the warmer end of the tube was collected. The solid was stirred in 100 mL of concentrated HCl for 15 min, and the ensuing mixture was filtered to give a deep amber filtrate. The remaining solid was treated again with successive aliquots of concentrated HCl (3×60 mL). The filtrates were combined, and an excess of Bu_4NBr (1 g, 3 mmol) was added, immediately inducing formation of an orange-brown precipitate. Solid NaHCO_3 was carefully added until the solution reached a pH of 3. The precipitate was collected by filtration, and washed with 80 mL of acetonitrile to give an orange filtrate. The solution was reduced to dryness using a rotary evaporator, and the solid residue was very quickly washed with 4 mL of acetonitrile. The solid was recrystallized by diffusing ether vapor into a concentrated acetonitrile solution, to give 0.17 g (25%) of product as red block-shaped crystals. Anal. Clad for $\text{C}_{32}\text{H}_{72}\text{Cl}_{12}\text{N}_2\text{O}_6\text{W}_6$: C, 18.22; H, 3.44; N, 1.33. Found: C, 18.62; H, 3.74; N, 1.20. Absorption spectrum (MeCN): λ_{max} (ϵ_{M}) 205 (45000), 221 (sh, 34000), 252 (26000), 273 (sh, 16000), 367 (9500), 436 (4400) nm. ES[−] MS: m/z 2109.89 ($\{(\text{Bu}_4\text{N})_2[\text{W}_6\text{O}_6\text{Cl}_{12}]\}^{1-}$), 1867.60 ($\{(\text{Bu}_4\text{N})[\text{W}_6\text{O}_6\text{Cl}_{12}]\}^{1-}$), 1830.62 ($\{(\text{Bu}_4\text{N})[\text{W}_6\text{O}_6\text{Cl}_{11}]\}^{1-}$), 1588.36 ($[\text{W}_6\text{O}_6\text{Cl}_{11}]^{1-}$).

$(\text{Bu}_4\text{N})_2[\beta\text{-W}_6\text{O}_6\text{Cl}_{12}]$. An ampule was charged with WOCl_4 (0.67 g, 2.0 mmol) and Bi (0.68 g, 3.2 mmol) in a dinitrogen atmosphere. The ampule was evacuated and sealed, and then heated in the manner described above for the synthesis of $(\text{Bu}_4\text{N})_2[\alpha\text{-W}_6\text{O}_6\text{Cl}_{12}]$. Treatment of the resulting black solid with HCl and Bu_4NBr also proceeded as described above. The ensuing dark brown solid was washed with successive aliquots of acetonitrile (6×3 mL). The dark brown-black filtrates obtained from the first three washes were combined, and 9 mL of ether was added to give a red-black precipitate. This precipitate was collected by filtration and set aside for use in the preparation of $(\text{Bu}_4\text{N})_3[\text{W}_6\text{O}_7\text{Cl}_{11}]$ (described below), while the orange filtrate was combined with the filtrates obtained from the final three of the aforementioned acetonitrile washes. By deconvoluting the electronic absorption spectrum over the range 335–550 nm, this solution was determined to contain a 5:7 mixture of $[\alpha\text{-W}_6\text{O}_6\text{Cl}_{12}]^{2-}$ and $[\beta\text{-W}_6\text{O}_6\text{Cl}_{12}]^{2-}$. Diffusion of ether into the solution over several days gave two types of large crystals: red block-shaped crystals of $(\text{Bu}_4\text{N})_2[\alpha\text{-W}_6\text{O}_6\text{Cl}_{12}]$ and red rhombic plate-shaped crystals of $(\text{Bu}_4\text{N})_2[\beta\text{-W}_6\text{O}_6\text{Cl}_{12}]$. The latter crystals were found to dissolve much more quickly upon addition of successive aliquots of acetonitrile (3×1 mL). The supernatant solutions were combined, and the crystallization/separation process was repeated twice to give 0.039 g (6%) of pure product, as confirmed by cyclic voltammetry and UV–vis spectroscopy. Anal. Clad for $\text{C}_{32}\text{H}_{72}\text{Cl}_{12}\text{N}_2\text{O}_6\text{W}_6$: C, 18.22; H, 3.44; N, 1.33. Found: C, 18.04; H, 3.32; N, 1.53. Absorption spectrum (MeCN): λ_{max} (ϵ_{M}) 204 (46000), 231 (29500), 249 (30800), 271 (sh, 16000), 385 (9100) nm. ES[−] MS: m/z 2109.87 ($\{(\text{Bu}_4\text{N})_2[\text{W}_6\text{O}_6\text{Cl}_{12}]\}^{1-}$), 1867.59 ($\{(\text{Bu}_4\text{N})[\text{W}_6\text{O}_6\text{Cl}_{12}]\}^{1-}$), 1830.62 ($\{(\text{Bu}_4\text{N})[\text{W}_6\text{O}_6\text{Cl}_{11}]\}^{1-}$), 1590.36 ($[\text{W}_6\text{O}_6\text{Cl}_{11}]^{1-}$).

$(\text{Bu}_4\text{N})_3[\text{W}_6\text{O}_7\text{Cl}_{11}]$. The red-black precipitate obtained in the preparation of $(\text{Bu}_4\text{N})_2[\beta\text{-W}_6\text{O}_6\text{Cl}_{12}]$ was recrystallized by diffusion of ether vapor into a concentrated acetonitrile solution. The product was obtained as 0.16 g (21%) of black cube-shaped crystals. Anal. Clad for $\text{C}_{48}\text{H}_{108}\text{Cl}_{11}\text{N}_3\text{O}_7\text{W}_6$: C, 24.72; H, 4.67; N, 1.80. Found: C, 24.49; H, 4.90; N, 1.70. Absorption spectrum (MeCN): λ_{max} (ϵ_{M}) 206 (48800), 235 (sh, 26900), 260 (sh, 16100), 290 (sh, 6880), 376 (6360), 550 (649)

- (7) Cordier, S.; Perrin, C.; Sergent, M. *Mater. Res. Bull.* **1996**, *31*, 683.
 (8) (a) Cordier, S.; Perrin, C.; Sergent, M. *Eur. J. Solid State Inorg. Chem.* **1994**, *31*, 1049. (b) Cordier, S.; Perrin, C.; Sergent, M. *Mater. Res. Bull.* **1997**, *32*, 25. (c) Anokhina, E. V.; Essig, M. W.; Lachgar, A. *Angew. Chem., Int. Ed. Engl.* **1998**, *37*, 522. (d) Anokhina, E. V.; Day, C. S.; Essig, M. W.; Lachgar, A. *Angew. Chem., Int. Ed.* **2000**, *39*, 1047. (e) Anokhina, E. V.; Day, C. S.; Essig, M. W.; Lachgar, A. *Inorg. Chem.* **2000**, *39*, 2185. (f) Gulo, F.; Perrin, C. *J. Mater. Chem.* **2000**, *10*, 1721. (g) Anokhina, E. V.; Day, C. S.; Lachgar, A. *Chem. Commun.* **2000**, 1491.
 (9) (a) Cordier, S.; Perrin, C.; Sergent, M. *J. Solid State Chem.* **1995**, *120*, 43. (b) Cordier, S.; Perrin, C.; Sergent, M. *Croat. Chem. Acta* **1995**, *68*, 781. (c) Ogliaro, F.; Cordier, S.; Halet, J.-F.; Perrin, C.; Saillard, J.-Y.; Sergent, M. *Inorg. Chem.* **1998**, *37*, 6199.
 (10) Cordier, S.; Gulo, F.; Perrin, C. *Solid State Sci.* **1999**, *1*, 637.
 (11) Dorman, W. C.; McCarley, R. E. *Inorg. Chem.* **1974**, *13*, 491.
 (12) Kolesnichenko, V.; Messerle, L. *Inorg. Chem.* **1998**, *37*, 3660.
 (13) (a) Morley, A. M. *J. Chem. Soc.* **1930**, 1987. (b) Crabtree, R. H.; Hlatky, G. G. *Polyhedron* **1985**, *4*, 521.

Table 1. Crystallographic Data^a and Structure Refinement Parameters for (Et₄N)₂[α-W₆O₆Cl₁₂], (Et₄N)₂[β-W₆O₆Cl₁₂], and (Et₄N)₃[W₆O₇Cl₁₁]

	(Et ₄ N) ₂ [α-W ₆ O ₆ Cl ₁₂]	(Et ₄ N) ₂ [β-W ₆ O ₆ Cl ₁₂]	(Et ₄ N) ₃ [W ₆ O ₇ Cl ₁₁]
formula	C ₁₆ H ₄₀ Cl ₁₂ N ₂ O ₆ W ₆	C ₁₆ H ₄₀ Cl ₁₂ N ₂ O ₆ W ₆	C ₂₄ H ₆₀ Cl ₁₁ N ₂ O ₇ W ₆
formula wt	1885.00	1885.00	1995.80
color	red	red	black
habit	irregular	block-shaped	block-shaped
T, K	155	163	147
space group	<i>P</i> $\bar{1}$	<i>P</i> 2 ₁ / <i>n</i>	<i>C</i> 2/ <i>c</i>
Z	4	4	4
a, Å	8.464(1)	11.6748(3)	19.545(4)
b, Å	22.526(2)	24.8097(8)	18.563(3)
c, Å	22.743(2)	14.5093(4)	13.422(2)
α, deg	118.684(4)		
β, deg	90.710(1)	113.120(1)	92.545(5)
γ, deg	91.511(4)		
V, Å ³	3801.3(7)	3865.1(2)	4865(2)
μ, mm ⁻¹	18.960	18.647	14.825
D _{calc} , g/cm ³	3.294	3.229	2.751
R1, wR2, b%	7.63, 20.05	2.26, 4.05	4.30, 7.79

^a Obtained with graphite monochromated Mo Kα (λ = 0.71073 Å) radiation. ^b R1 = Σ||F_o - |F_c||/Σ|F_o|; wR2 = {Σ[w(|F_o - |F_c||)²]/Σ[w(|F_o|)²]}^{1/2}.

nm. ES⁻ MS: *m/z* 2088.89 ((Bu₄N)₂[W₆O₇Cl₁₁]¹⁻), 1811.64 ((Bu₄N)[W₆O₇Cl₁₀]¹⁻), 1534.39 ([W₆O₇Cl₉]¹⁻).

X-ray Structure Determinations. The foregoing preparations were repeated using Et₄NCl in place of Bu₄NBr in order to generate high-quality crystals without extensive disorder of the counterions. Crystals suitable for X-ray analysis were obtained for (Et₄N)₂[α-W₆O₆Cl₁₂] and (Et₄N)₂[β-W₆O₆Cl₁₂] by slow evaporation of acetonitrile solutions, and for (Et₄N)₃[W₆O₇Cl₁₁] by diffusing ether into a concentrated acetonitrile solution.

The crystals were coated in Paratone-N oil, attached to quartz fibers, transferred to a Siemens SMART diffractometer, and cooled in a dinitrogen stream. Lattice parameters were initially determined from a least-squares analysis of more than 100 centered reflections; these parameters were later refined against all data. None of the crystals showed significant decay during data collection. The raw intensity data were converted (including corrections for background, Lorentz, and polarization effects) to structure factor amplitudes and their esd's using the SAINT 4.15 program. An empirical absorption correction was applied to each data set using SADABS. Space group assignments were based on systematic absences, *E*-statistics, and successful refinement of the structures. Structures were solved by direct methods with the aid of difference Fourier maps and were refined against all data using the SHELXTL 5.0 software package. Crystallographic parameters are listed in Table 1.

In all structures, hydrogen atoms were inserted at idealized positions and refined using a riding model with an isotropic thermal parameter 1.2 times that of the attached carbon atom (1.5 times for methyl hydrogens). Thermal parameters for all non-hydrogen atoms were refined anisotropically, with the following exceptions. Six of the twelve independent oxygen atoms and all carbon and nitrogen atoms in the structure of (Et₄N)₂[β-W₆O₆Cl₁₂] were refined isotropically. Two oxygen atoms and four carbon atoms in the structure of (Et₄N)₃[W₆O₇Cl₁₁] were also refined isotropically. These two oxygen atoms were each found in crystallographically distinct clusters to be disordered over four different edge-bridging sites; the chlorine atoms associated with these sites were refined with an occupancy of 0.75, accordingly. The position of one of the disordered oxygen atoms was refined without constraints, while the other was constrained to be 1.90 ± 0.03 Å away from the neighboring tungsten atoms. The somewhat high final agreement factors obtained for the structure of (Et₄N)₂[α-W₆O₆Cl₁₂] (see Table 1) are attributed to the poor quality and small size of the crystal.

Other Physical Measurements. Electronic absorption spectra were obtained using a Hewlett-Packard 8453 spectrophotometer. Electrochemical measurements were conducted with a Bioanalytical Systems CV-50 potentiostat with platinum-disk working, platinum-wire auxiliary, and silver-wire reference electrodes. Samples were measured at a scan

rate of 100 mV/s in 0.1 M (Bu₄N)(BF₄) supporting electrolyte, and ferrocene (Fc) was added after each measurement as an internal reference. Mass spectrometric measurements were performed in the negative ion mode on a Brüker Apex II 7 T actively shielded FT-ICR mass spectrometer equipped with an analytical electrospray ion source instrument.

Electronic Structure Calculations. Density functional theory calculations were performed for both isomers of [W₆O₆Cl₁₂]²⁻, using the Gaussian 98 quantum chemistry software package.¹⁴ Idealized geometries with full *D*_{3d} symmetry were assumed. Single-point energies were calculated using B3LYP functionals¹⁵ and the LANL2DZ effective core potentials (which included relativistic effects for tungsten atoms but not for chlorine atoms) with the corresponding Gaussian basis sets.¹⁶

Results and Discussion

Syntheses. The synthesis of the solid precursor to (Bu₄N)₂[α-W₆O₆Cl₁₂] parallels the method recently employed in a high-yield synthesis of W₆Cl₁₂ (reaction 1).¹² Replacing WCl₆ with WOCl₄, a W₆O₆Cl₁₀ parent phase with 14 metal-based valence electrons per cluster is targeted according to the following reaction.



The BiCl₃ is sublimed away, leaving a black solid product that is amorphous by powder X-ray diffraction. While the precise nature of the amorphous solid is unknown, it likely exhibits an extended [W₆O₆Cl₆Cl₆]^{a-4/2} connectivity¹⁷ with μ₂-Cl atoms bridging between cluster units (as observed in the ordered two-dimensional frameworks of W₆Cl₁₂¹⁸ and Li₂Nb₆Cl₁₆¹⁹). Regardless, the clusters are excised from the solid by reaction with concentrated HCl, to give [α-W₆O₆Cl₁₂]²⁻ as the only soluble product. The low overall reaction yield may be attributed to the fact that much of this solid remains undissolved. Metathesis with Bu₄NBr then provides (Bu₄N)₂[α-W₆O₆Cl₁₂], a form of the cluster that is soluble in polar organic solvents. The low temperature (360 °C) at which the reduction of WOCl₄ is carried out suggests that the strong W–O bonds could potentially be preserved during the course of reaction 2. Consistent with this notion, the ensuing cluster product contains just one oxygen atom per tungsten atom. Indeed, longer reaction times and higher temperatures appear to favor disproportionation to a product containing face-capped octahedral [W₆Cl₈]⁴⁺ cluster cores and unidentified tungsten oxide phases.

- (14) Frisch, M. J.; Trucks, G. W.; Schlegel, H. B.; Scuseria, G. E.; Robb, M. A.; Cheeseman, J. R.; Zakrzewski, V. G.; Montgomery, J. A.; Stratmann, R. E.; Burant, J. C.; Dapprich, S.; Millam, J. M.; Daniels, A. D.; Kudin, K. N.; Strain, M. C.; Farkas, O.; Tomasi, J.; Barone, V.; Cossi, M.; Cammi, R.; Mennucci, B.; Pomelli, C.; Adamo, C.; Clifford, S.; Ochterski, J.; Petersson, G. A.; Ayala, P. Y.; Cui, Q.; Morokuma, K.; Malick, D. K.; Rabuck, A. D.; Raghavachari, K.; Foresman, J. B.; Cioslowski, J.; Ortiz, J. V.; Stefanov, B. B.; Liu, G.; Liashenko, A.; Piskorz, P.; Komaromi, I.; Gomperts, R.; Martin, R. L.; Fox, D. J.; Keith, T.; Al-Laham, M. A.; Peng, C. Y.; Nanayakkara, A.; Gonzalez, C.; Challacombe, M.; Gill, P. M. W.; Johnson, B. G.; Chen, W.; Wong, M. W.; Andres, J. L.; Head-Gordon, M.; Replogle, E. S.; Pople, J. A. *Gaussian 98*, Revision A.7; Gaussian, Inc.: Pittsburgh, PA, 1998.
- (15) (a) Vosko, S. H.; Wilk, L.; Nusair, M. *Can. J. Phys.* **1980**, *58*, 1200. (b) Becke, A. D. *J. Chem. Phys.* **1993**, *98*, 5648. (c) Lee, C.; Yang, W.; Parr, R. G. *Phys. Rev. B* **1988**, *37*, 785.
- (16) (a) Hay, P. J.; Wadt, W. R. *J. Chem. Phys.* **1985**, *82*, 270. (b) Wadt, W. R.; Hay, P. J. *J. Chem. Phys.* **1985**, *82*, 284. (c) Hay, P. J.; Wadt, W. R. *J. Chem. Phys.* **1985**, *82*, 299. (d) Dunning, T. H., Jr.; Hay, P. J. In *Modern Theoretical Chemistry*; Schaefer, H. F., III, Ed.; Plenum: New York, 1976; Vol. 3, p 1.
- (17) Nomenclature: Schäfer, H.; Schnering, H.-G. *Angew. Chem.* **1964**, *76*, 833. See also ref 1c.
- (18) Schäfer, H.; von Schnering, H.-G.; Tillack, J.; Kuhnen, F.; Wöhrle, F.; Baumann, H. *Z. Anorg. Allg. Chem.* **1967**, *353*, 281.
- (19) Bajan, B.; Meyer, H.-J. *Z. Anorg. Allg. Chem.* **1997**, *623*, 791.

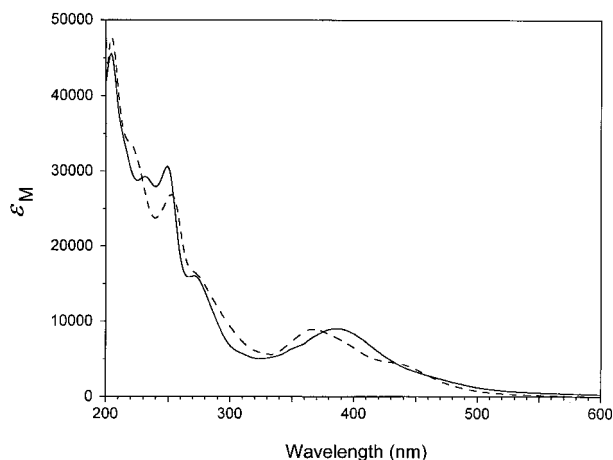


Figure 2. Electronic absorption spectra for $(\text{Bu}_4\text{N})_2[\alpha\text{-W}_6\text{O}_6\text{Cl}_{12}]$ (dashed line) and $(\text{Bu}_4\text{N})_2[\beta\text{-W}_6\text{O}_6\text{Cl}_{12}]$ (solid line) in acetonitrile.

Reactions employing a higher ratio of bismuth metal were undertaken in an effort to further reduce the tungsten centers, and perhaps push the cluster product toward a face-capped octahedral geometry. The soluble products were instead discovered to consist of a mixture of hexanuclear oxochloride clusters with tungsten still in the +3.67 oxidation state. Separation of the $[\text{W}_6\text{O}_7\text{Cl}_{11}]^{3-}$ cluster was carried out by exploiting the lower solubility of its Bu_4N^+ salt in a mixture of acetonitrile and ether. The remaining solution was ultimately determined to contain two distinct isomers of $[\text{W}_6\text{O}_6\text{Cl}_{12}]^{2-}$: the previously observed α isomer and an additional β isomer not present in the soluble components of reaction 2. As shown in Figure 2, the isomers can be distinguished by their slightly different electronic absorption spectra. By fitting the absorption spectrum to a linear combination of the spectra for the pure isomers, the solution was found to contain a 5:7 mixture of the α and β isomers. Upon crystallization, the isomers segregate into large crystals of $(\text{Bu}_4\text{N})_2[\alpha\text{-W}_6\text{O}_6\text{Cl}_{12}]$ and $(\text{Bu}_4\text{N})_2[\beta\text{-W}_6\text{O}_6\text{Cl}_{12}]$ with very different morphologies. The α isomer forms large block-shaped crystals, while the β isomer forms thin rhombic plate-shaped crystals. The greater surface area-to-volume ratio of the latter crystals causes them to dissolve much more quickly in acetonitrile, permitting separation of the isomers via successive dissolution/crystallization steps. The overall yield of pure $(\text{Bu}_4\text{N})_2[\beta\text{-W}_6\text{O}_6\text{Cl}_{12}]$ is only 6%, in part owing to this rather inefficient separation process.

Structures. Single crystals obtained directly from the reaction products exhibited extensive disorder of the Bu_4N^+ cations. The analogous Et_4N^+ salts were therefore synthesized to acquire reliable crystal structures. As might be anticipated for a count of 14 metal-based valence electrons, the $[\text{W}_6\text{O}_6\text{Cl}_{12}]^{2-}$ and $[\text{W}_6\text{O}_7\text{Cl}_{11}]^{3-}$ clusters all exhibit structures based on the edge-bridged octahedral geometry (see Figure 1).

Figure 3 depicts the structure of the $[\alpha\text{-W}_6\text{O}_6\text{Cl}_{12}]^{2-}$ cluster, in which the edges of the W_6 octahedron are bridged by six oxygen atoms and six chlorine atoms. The oxygen atoms are situated on the edges between two opposing triangular faces, resulting in a compression of the octahedron along a 3-fold rotation axis. Selected mean interatomic distances and angles for the D_{3d} -symmetry cluster are listed in Table 2. The mean core $\text{W}-\text{Cl}$ distance of 2.453(7) Å and mean $\text{W}-\text{W}$ distance of 2.914(5) Å for the associated edges are marginally longer than those in W_6Cl_{18} (2.39(2) and 2.878(4) Å, respectively),³ perhaps owing to the different number of valence electrons. The much shorter mean $\text{W}-\text{O}$ bond distance of 1.89(3) Å is accompanied by a shorter mean $\text{W}-\text{W}$ distance of 2.693(3) Å

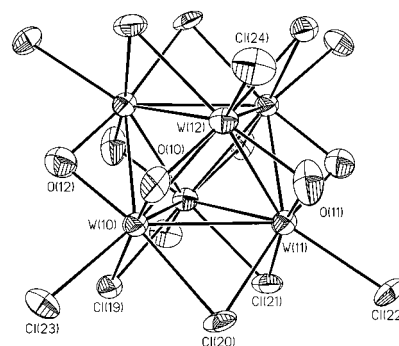


Figure 3. Structure of the trigonally compressed $[\alpha\text{-W}_6\text{O}_6\text{Cl}_{12}]^{2-}$ cluster, as observed in $(\text{Et}_4\text{N})_2[\alpha\text{-W}_6\text{O}_6\text{Cl}_{12}]$; ellipsoids are drawn at the 60% probability level. The cluster resides on a crystallographic inversion center.

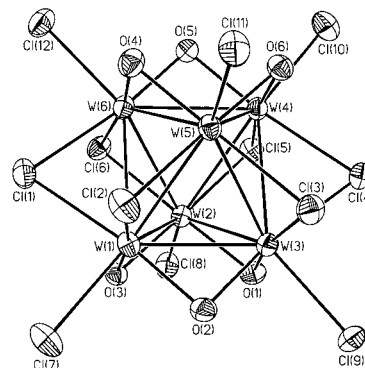


Figure 4. Structure of the trigonally elongated $[\beta\text{-W}_6\text{O}_6\text{Cl}_{12}]^{2-}$ cluster, as observed in $(\text{Et}_4\text{N})_2[\beta\text{-W}_6\text{O}_6\text{Cl}_{12}]$; ellipsoids are drawn at the 60% probability level.

Table 2. Selected Mean Interatomic Distances (Å) and Angles (deg) for the Clusters in the Structures of $(\text{Et}_4\text{N})_2[\alpha\text{-W}_6\text{O}_6\text{Cl}_{12}]$, $(\text{Et}_4\text{N})_2[\beta\text{-W}_6\text{O}_6\text{Cl}_{12}]$, $(\text{Et}_4\text{N})_3[\text{W}_6\text{O}_7\text{Cl}_{11}]$, and $\text{W}_6\text{Cl}_{18}\cdot 4\text{Me}_2\text{SO}^{3b}$

	$[\alpha\text{-W}_6\text{O}_6\text{Cl}_{12}]^{2-}$	$[\beta\text{-W}_6\text{O}_6\text{Cl}_{12}]^{2-}$	$[\text{W}_6\text{O}_7\text{Cl}_{11}]^{3-a}$	W_6Cl_{18}
$\text{W}-\text{W}^b$	2.693(3)	2.704(2)	2.692(4)	
$\text{W}-\text{W}^c$	2.914(5)	2.889(9)	2.869	2.878(4)
$\text{W}-\text{O}$	1.89(3)	1.907(5)	1.90(2)	
$\text{W}-\text{Cl}^d$	2.453(7)	2.45(1)	2.45(2)	2.39(2)
$\text{W}-\text{Cl}^a$	2.41(1)	2.408(4)	2.433(3)	2.447(6)
$\text{W}-\text{W}-\text{W}^d$	65.5(1)	55.8(1)	56.28(4)	
$\text{W}-\text{O}-\text{W}$	91(2)	90.3(2)	90.3(9)	
$\text{W}-\text{Cl}-\text{W}$	72.9(2)	72.2(3)	71.3(2)	74.0(3)
$\text{O}-\text{W}-\text{O}$	95(2)	95.8(7)	94.9(1)	
$\text{O}-\text{W}-\text{Cl}^d$	89(1)	88.7(8)	88.9(8)	
$\text{O}-\text{W}-\text{Cl}^a$	87(1)	86.2(8)	86.8(5)	
$\text{Cl}^d-\text{W}-\text{Cl}^d$	85.2(7)	85.6(5)	85.9(6)	88.5(5)
$\text{Cl}^d-\text{W}-\text{Cl}^a$	85.5(7)	85.5(8)	84.6(8)	

^a Excluding parameters associated with the disordered O atom.

^b Along an edge bridged by an O atom. ^c Along an edge bridged by a Cl atom. ^d Unique angle within the isosceles W_3 triangles.

for the oxo-bridged edges of the octahedron. These are comparable to the corresponding mean distances of 2.00(2) and 2.69(2) Å observed for the $[\text{W}_6\text{O}_{12}]^{2-}$ cores in $\text{Sn}_{10}\text{W}_{16}\text{O}_{44}$.⁶ Both types of $\text{W}-\text{W}$ bonds in $[\alpha\text{-W}_6\text{O}_6\text{Cl}_{12}]^{2-}$ are longer than those occurring in the face-capped octahedral $[\text{W}_6\text{Cl}_{14}]^{2-}$ cluster (mean $\text{W}-\text{W} = 2.607(4)$ Å)²⁰ with 24 metal-based valence electrons.

The structure of $[\beta\text{-W}_6\text{O}_6\text{Cl}_{12}]^{2-}$ (Figure 4) differs from that of $[\alpha\text{-W}_6\text{O}_6\text{Cl}_{12}]^{2-}$ primarily in the arrangement of its core

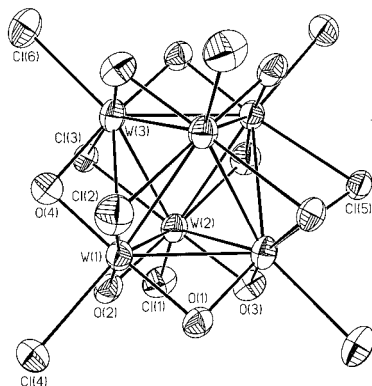


Figure 5. Structure of the $[\text{W}_6\text{O}_7\text{Cl}_{11}]^{3-}$ cluster, as observed in $(\text{Et}_4\text{N})_3[\text{W}_6\text{O}_7\text{Cl}_{11}]$; ellipsoids are drawn at the 30% probability level. The cluster resides on a crystallographic inversion center. Only one of the two possible locations for O(4) in the asymmetric unit is shown; the other equally likely location is bridging the W(2)–W(3) edge of the W_6 octahedron. Note that only one enantiomer of the chiral C_2 -symmetry cluster is depicted.

oxygen and chlorine atoms. The positions of these atoms have been interchanged, such that the chlorine atoms rather than the oxygen atoms are situated on the edges between two opposing triangular faces of the W_6 octahedron. Thus, the shorter W–W bonds associated with the oxo-bridged edges on opposing faces result in an elongation of the octahedron along a 3-fold rotation axis. Selected mean distances and angles for the cluster, which also exhibits D_{3d} symmetry, are listed in Table 2 for comparison. Inspection of the two sets of geometric parameters reveals a close match between the α and β isomers, the fundamental distinction—the nature of the distortion of the W_6 octahedron—only becoming apparent with the different W–W–W angles.

At least formally, the structure of $[\text{W}_6\text{O}_7\text{Cl}_{11}]^{3-}$ (Figure 5) is derived from that of $[\beta\text{-W}_6\text{O}_6\text{Cl}_{12}]^{2-}$ by substitution of an O^{2-} ion for a Cl^- ion in the cluster core. In the crystal structure of $(\text{Et}_4\text{N})_3[\text{W}_6\text{O}_7\text{Cl}_{11}]$, the additional oxygen atom is disordered over just four of the six edge sites located around the waist of the elongated W_6 octahedron. The distances associated with these four edges (W(1)–W(3) = 2.848(1) Å and W(2)–W(3) = 2.846(1) Å) are slightly shorter than the remaining two strictly chloro-bridged edge distances (W(1)–W(2') = 2.869(1) Å). Table 2 again lists a selection of mean interatomic distances and angles. Only minor deviations from the parameters observed in the $[\beta\text{-W}_6\text{O}_6\text{Cl}_{12}]^{2-}$ cluster are apparent. Most notably, the terminal W–Cl bonds are slightly longer in the trianionic cluster, consistent with its less-positive core charge. As isolated from the above preparation, the compound $(\text{Bu}_4\text{N})_3[\text{W}_6\text{O}_7\text{Cl}_{11}]$ contains exclusively the isomer shown in Figure 5. However, a solitary piece of evidence supporting the existence of a second isomer of $[\text{W}_6\text{O}_7\text{Cl}_{11}]^{3-}$, in which an O^{2-} ion is substituted for a Cl^- ion in the core of $[\alpha\text{-W}_6\text{O}_6\text{Cl}_{12}]^{2-}$, was obtained with the crystallographic analysis of a compound of apparent formula $(\text{Et}_4\text{N})_6[\alpha\text{-W}_6\text{O}_7\text{Cl}_{11}][\beta\text{-W}_6\text{O}_7\text{Cl}_{11}]$.²¹ We speculate that the $[\text{W}_6\text{O}_7\text{Cl}_5]^{3+}$ cluster core may form from a $[\text{W}_6\text{O}_6\text{Cl}_6]^{4+}$ core via a ligand exchange reaction occurring in the solid flux, and that the predominance of the isomer depicted in Figure 5 may therefore be related to the greater amount of the β isomer of $[\text{W}_6\text{O}_6\text{Cl}_{12}]^{2-}$ produced in the synthesis.

(21) Poor quality data were obtained at 156 K, leading to a crudely refined structure associated with the following unit cell for $(\text{Et}_4\text{N})_6[\alpha\text{-W}_6\text{O}_7\text{Cl}_{11}][\beta\text{-W}_6\text{O}_7\text{Cl}_{11}]$: $R3$, $a = 18.84(2)$ Å, $c = 22.88(4)$ Å, $V = 7032(16)$ Å³, $Z = 3$. The presence of exclusively $[\text{W}_6\text{O}_7\text{Cl}_{11}]^{3-}$ clusters in this crystal was confirmed by mass spectrometry.

Table 3. Number^a of Isomers for Edge-Bridged Octahedral $\text{W}_6\text{O}_n\text{Cl}_{12-n}$ Cluster Cores

core formula	total isomers	chiral isomers
$\text{W}_6\text{OCl}_{11}$, $\text{W}_6\text{O}_{11}\text{Cl}$	1	0
$\text{W}_6\text{O}_2\text{Cl}_{10}$, $\text{W}_6\text{O}_{10}\text{Cl}_2$	4	1
$\text{W}_6\text{O}_3\text{Cl}_9$, $\text{W}_6\text{O}_9\text{Cl}_3$	9	4
$\text{W}_6\text{O}_4\text{Cl}_8$, $\text{W}_6\text{O}_8\text{Cl}_4$	18	9
$\text{W}_6\text{O}_5\text{Cl}_7$, $\text{W}_6\text{O}_7\text{Cl}_5$	24	15
$\text{W}_6\text{O}_6\text{Cl}_6$	30	18

^a Pairs of enantiomers were counted as just one isomer.

The possible isomers for an edge-bridged octahedral $\text{W}_6\text{O}_n\text{Cl}_{12-n}$ cluster core, or, indeed, for any mixed-ligand $\text{M}_6\text{X}_n\text{Y}_{12-n}$ core adopting this geometry, are enumerated in Table 3. The structures assumed by $[\alpha\text{-W}_6\text{O}_6\text{Cl}_{12}]^{2-}$ and $[\beta\text{-W}_6\text{O}_6\text{Cl}_{12}]^{2-}$ represent just two of the thirty possibilities for a $[\text{W}_6\text{O}_6\text{Cl}_6]^{4+}$ core. Of these thirty isomers, twenty-three are consistent with a condensation-type mechanism that preserves all of the W–O bonds in six WOCl_4 precursor molecules. Significantly, the two observed D_{3d} -symmetry structures correspond to the only two ways of distorting the W_6 octahedron to give six equivalent short (oxo-bridged) and six equivalent long (chloro-bridged) W–W bonds. A total of twenty-four different isomers are possible for a $[\text{W}_6\text{O}_7\text{Cl}_5]^{3+}$ core, such as present in the $[\text{W}_6\text{O}_7\text{Cl}_{11}]^{3-}$ cluster. Assuming no external oxygen source, the formation of any of these isomers would obviously require cleavage of the W–O moiety in at least one WOCl_4 species per cluster produced.

Electrochemistry. Cyclic voltammetry provided an early indication that more than one isomer of the $[\text{W}_6\text{O}_6\text{Cl}_{12}]^{2-}$ cluster was present in solutions produced from reactions incorporating additional bismuth metal. A cyclic voltammogram of a crude solution obtained after separation of the $[\text{W}_6\text{O}_7\text{Cl}_{11}]^{3-}$ cluster is shown at the top in Figure 6. This clearly represents a superposition of the cyclic voltammograms for pure $[\alpha\text{-W}_6\text{O}_6\text{Cl}_{12}]^{2-}$ (Figure 6, bottom) and $[\beta\text{-W}_6\text{O}_6\text{Cl}_{12}]^{2-}$ (Figure 6, middle), with a slightly greater concentration of the latter. Each isomer exhibits two reversible reduction waves corresponding to $[\text{W}_6\text{O}_6\text{Cl}_{12}]^{2-/-3-}$ and $[\text{W}_6\text{O}_6\text{Cl}_{12}]^{3-/-4-}$ couples. Relative to Fc/Fc^+ , these couples are centered at $E_{1/2} = -0.26$ V ($\Delta E_p = 70$ mV) and $E_{1/2} = -1.06$ V ($\Delta E_p = 65$ mV) for $[\alpha\text{-W}_6\text{O}_6\text{Cl}_{12}]^{2-}$, and at $E_{1/2} = -0.41$ V ($\Delta E_p = 74$ mV) and $E_{1/2} = -1.14$ V ($\Delta E_p = 72$ mV) for $[\beta\text{-W}_6\text{O}_6\text{Cl}_{12}]^{2-}$. Thus, for both couples, the α isomer of the cluster is slightly easier to reduce than the β isomer. No reversible oxidation events were observed for either isomer.

The cyclic voltammogram of $[\text{W}_6\text{O}_7\text{Cl}_{11}]^{3-}$ in acetonitrile (Figure 7) reveals just one reversible reduction wave. This corresponds to a $[\text{W}_6\text{O}_7\text{Cl}_{11}]^{3-/-4-}$ couple centered at $E_{1/2} = -1.17$ V ($\Delta E_p = 77$ mV) relative to Fc/Fc^+ . A second irreversible reduction event occurs at approximately -1.9 V. The shift of the reduction waves to potentials that are more negative than those observed for $[\beta\text{-W}_6\text{O}_6\text{Cl}_{12}]^{2-}$ is consistent with the increased negative charge of the cluster. Again, no reversible oxidation event was observed.

Electronic Structures. Density functional theory calculations were employed to probe the electronic structures of both isomers of the $[\text{W}_6\text{O}_6\text{Cl}_{12}]^{2-}$ cluster. Energy level diagrams within the vicinity of the frontier orbitals are displayed in Figure 8 for comparison. Both diagrams exhibit a sizable HOMO–LUMO gap of more than 2 eV, leading to diamagnetic electron configurations. The two isomers are calculated to be virtually identical in total energy, with the β isomer structure lying just 1.4 kcal/mol below the α isomer structure. For each isomer,

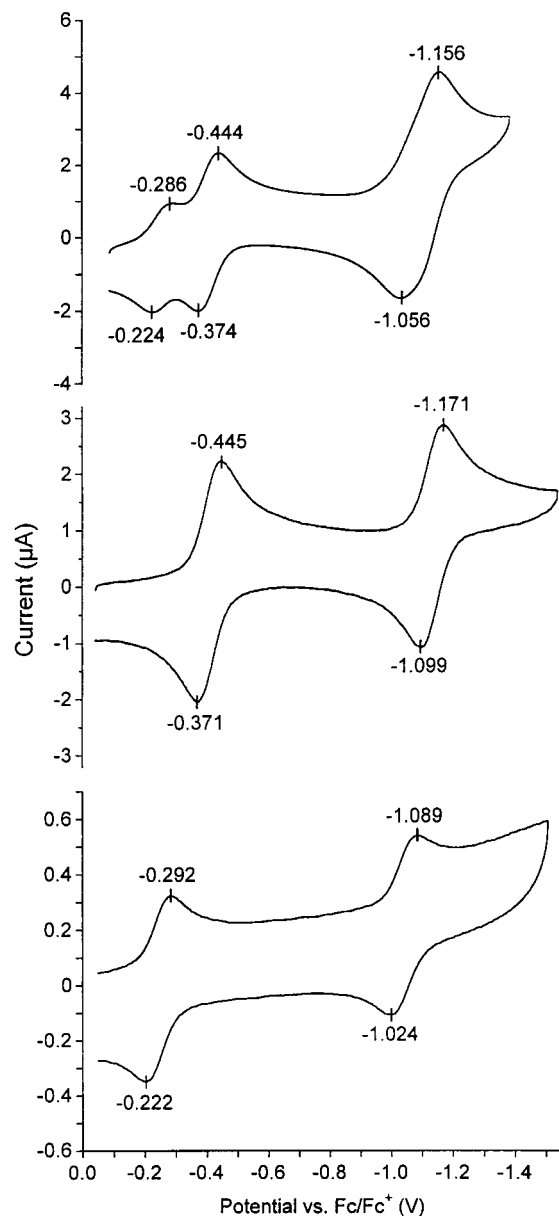


Figure 6. Cyclic voltammograms of acetonitrile solutions containing a mixture of $[\alpha\text{-W}_6\text{O}_6\text{Cl}_{12}]^{2-}$ and $[\beta\text{-W}_6\text{O}_6\text{Cl}_{12}]^{2-}$ (top), pure $[\beta\text{-W}_6\text{O}_6\text{Cl}_{12}]^{2-}$ (middle), and pure $[\alpha\text{-W}_6\text{O}_6\text{Cl}_{12}]^{2-}$ (bottom).

the W–W bonding character is not restricted to just the seven highest-energy occupied orbitals (as might be expected for a cluster with fourteen metal-based valence electrons), but, owing to interactions with lone pair orbitals on the terminal chloride ligands, extends to include another six lower-energy occupied orbitals. The a_{1g} HOMO of the α isomer and the pair of e_g HOMOs of the β isomer are all a combination of W–W σ -bonding and W–Cl $^\pi$ π -antibonding in character. The LUMOs, which correspond to a_{1g} and e_u orbitals for the α and β isomers, respectively, are all primarily W-based and essentially non-bonding in character. The LUMO of the α isomer is calculated to be slightly lower in energy than that of the β isomer, consistent with the α isomer being more easily reduced (see Figure 6). However, it was not determined if these LUMOs are indeed the additional orbitals occupied in the reduced forms of the clusters. More detailed information concerning the atomic contributions to the frontier orbitals for both isomers is supplied in Tables S-16 and S-17 of the Supporting Information.

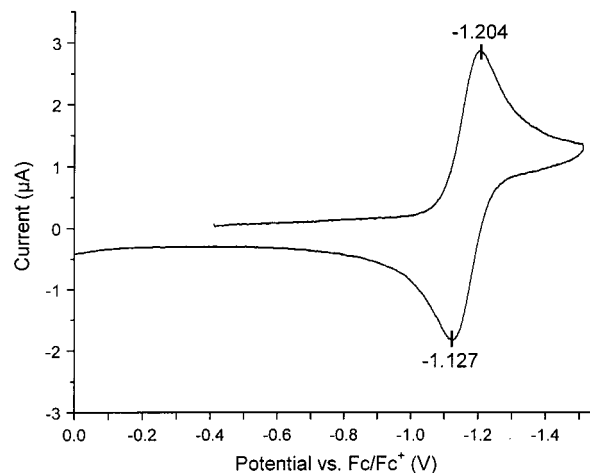


Figure 7. Cyclic voltammogram of a solution of $(\text{Bu}_4\text{N})_3[\text{W}_6\text{O}_7\text{Cl}_{11}]$ in acetonitrile.

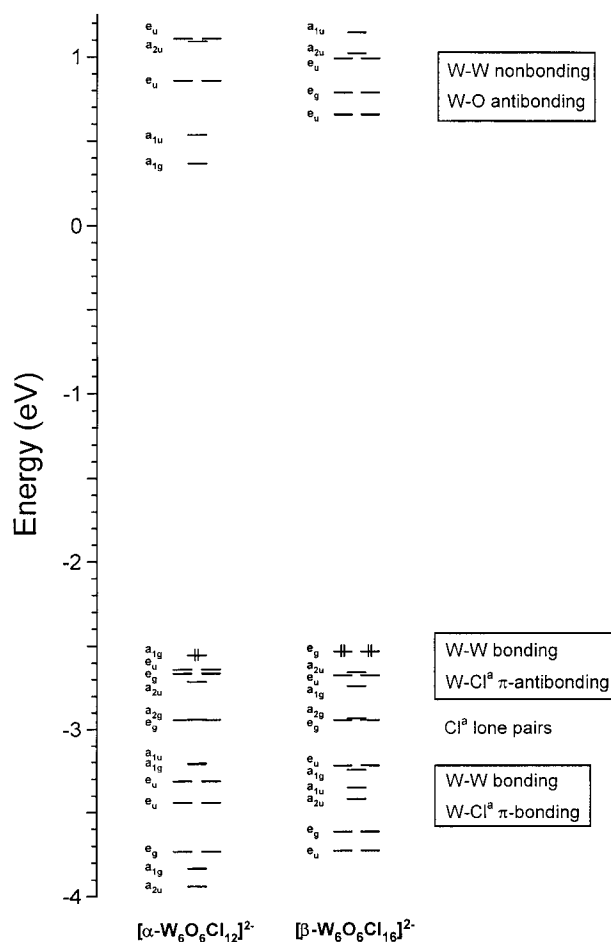


Figure 8. Energy level diagrams for the two isomers of $[\text{W}_6\text{O}_6\text{Cl}_{12}]^{2-}$ with idealized D_{3d} symmetry, as calculated using density functional theory. Electrons fill up through the indicated orbitals.

Outlook

Reaction 2 above may exemplify a general reaction type for producing a range of new transition metal oxohalide clusters. Cluster products exhibiting a 1:1 metal/oxygen ratio could potentially be achieved through similar low-temperature reductions of, for example, MOX_3 ($M = \text{Nb, Ta; X} = \text{F, Cl, Br, I}$) and MOX_4 ($M = \text{Mo, W, Re; X} = \text{F, Cl, Br}$). Analogous reactions employing MO_2X ($M = \text{Nb, Ta; X} = \text{F, Cl, Br, I}$) or MO_2X_2 ($M = \text{Mo, W; X} = \text{F, Cl, Br, I}$) species may afford

clusters with a 1:2 metal/oxygen ratio. Other metal/oxygen ratios might be attained with more complex reactions involving mixtures of metal halide and metal oxohalide reactants. We are currently pursuing several of these avenues of investigation.

Acknowledgment. This research was funded by the University of California, the Petroleum Research Fund (administered by the ACS), and the Camille and Henry Dreyfus Foundation. We thank the Department of Defense for supplying a fellowship to N.R.M.C. and Dr. Jorge Rodriguez for many helpful discussions.

Supporting Information Available: X-ray structural information for the compounds listed in Table 1, including tables of crystal and refinement data, atomic positional and thermal parameters, and interatomic distances and angles; tables of atomic contributions to the frontier orbitals obtained from density functional theory calculations performed on $[\alpha\text{-W}_6\text{O}_6\text{Cl}_{12}]^{2-}$ and $[\beta\text{-W}_6\text{O}_6\text{Cl}_{12}]^{2-}$; and an X-ray crystallographic file (CIF). This material is available free of charge via the Internet at <http://pubs.acs.org>.

IC0013734